ACTIVE CANCELLATION OF TOLLMIEN-SCHLICHTING INSTABILITIES UP TO M = 0.40

Marcus Engert, Wolfgang Nitsche
Institute of Aero- and Astronautics, Berlin Institute of Technology

Keywords: *active control, laminar flow control, Tollmien-Schlichting waves, compressible flows, sensor-actuator systems*

Abstract

The laminar-turbulent transition of a boundary layer can be delayed by active and passive methods. Active control methods, which are applied at TU Berlin, directly interact with the instability waves (Tollmien-Schlichting (TS) waves) of the laminar boundary layer. This active wave cancellation (AWC) method is based on the wave superposition principle, i.e. the superposition of artificially generated anti-waves on naturally occurring disturbances. The energy consumption of this method is considerably lower than the stabilization by manipulation of the local mean velocity profile, e.g. by boundary layer suction. This paper reports on AWC experiments performed in the TU Berlin transonic wind tunnel using a modified unswept NACA 0004 wing section at Mach numbers ranging from 0.2 to 0.4.

1 Introduction

The delay of the laminar-turbulent transition is crucial for skin friction reduction. Many active and passive methods were investigated in this field. Most control techniques are aimed at stabilizing the mean velocity profile of the boundary layer, whereas the wave-cancellation method assumes that a wavelike disturbance can be cancelled by introducing another wave with a similar amplitude but opposite in phase. Since TS waves are the main reason for laminar-turbulent transition on unswept wings, the active cancellation of these harmonic perturbations is the most efficient way to delay transition. Based on the linear superposition principle, the evolution and spatial amplification of TS waves can be suppressed by an active skin consisting of sensors, actuators and controllers. This application is useful for TS waves in their early linear stage up to the weak non-linear stage, especially if they are dominated by two-dimensional TS modes. This type of TS scenario may also be found on a swept wing in the mid-chord region, if cross-flow instabilities were previously suppressed, e.g. by suction in the leading-edge region.

For many years an adaptive linear control algorithm has been successfully used to attenuate TS instabilities on an unswept wing at TU Berlin [1, 4, 5]. The principle approach is shown in Fig. 1.

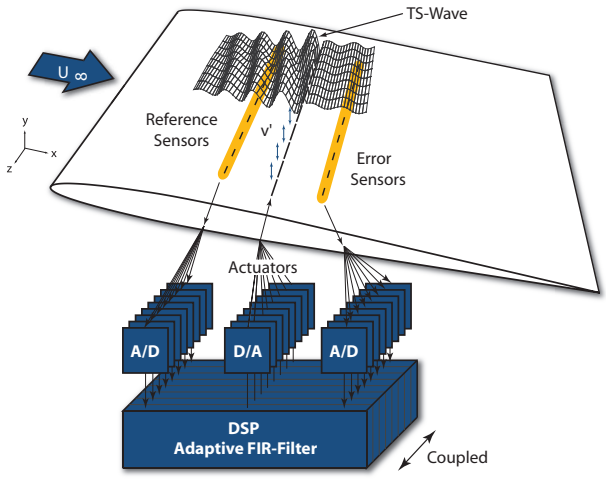

Fig. 1 Principle of an active wave control system [5]

The convective TS waves are detected by a reference-sensor upstream of the actuator. The actuator signal to excite the cancelling wave is generated by applying an adaptive transfer function (adaptive digital filter) to the disturbance signal of the reference-sensor. The filter is continuously adapted in order to minimize the signal power of the error-sensor located downstream. The adaptation process is performed in real time by a digital signal processor, which executes an adaptive filtered-x-LMS (FxLMS) algorithm, originally introduced by Burgess [2] and Widrow et al. [6].

It is a well known fact that a complete cancellation of TS Instabilities is impossible. Just a few reasons for this are technical limits due to the signal-to-noise ratio of the sensors, nonlinear characteristics of the actuator or weak nonlinearities of the TS waves between the reference- and error-sensor. Therefore, a multiple channel system in span-wise and flow direction is required, which is beyond the scope of this paper.

2 Experimental Set-Up

The experiments were conducted in an Eiffel-type low-turbulence wind tunnel between M = 0.2 and 0.4. The wind tunnel's cross section size is 150 mm x 150 mm at the inlet of the test section, and has a length of 990 mm. Adjustable top and bottom fibre-glass walls of the test section can be individually deflected by 13 computer-controlled servo-motors. This allows artificial/controlled pressure gradients along the wing profile to be introduced in order stabilize or destabilize the natural transition process. Hence, transition could be positioned in the vicinity of the sensor/actuator system, independent of the free-stream Mach numbers. Consequently, just one single model was necessary for testing a variety of Mach numbers. The contraction ratio of 47:1 between the settling chamber and the test section inlet yields a free-stream turbulence intensity of less than 0.15%, which makes this wind tunnel ideally suited for experiments concerning active cancellation of naturally occurring TS instabilities.

The unswept test wing has a modified NACA 0004 profile at the leading edge. At its maximum thickness of 30 mm the NACA nose is tangentially extended with a flat plate and ends with a flap at the trailing edge (chord c = 750 mm), Fig. 2a. The highly polished aluminium profile is equipped with a rectangular opening located at $0.1 \leq x/c \leq 0.6$ from the model's leading edge for the installation of different sensor-actuator arrangements depending on the experimental configuration. The pressure distribution is instantaneously measured by 18 equidistantly arranged pressure orifices in the flow direction. The model is horizontally fixed 5 mm below the centre of the two-dimensional adaptive test section to reduce blockage effects on the model's sensor side at higher Mach numbers.

One plate insert (Fig. 2b) consists of an array of surface hot wires (SHW) which are symmetrically aligned to the centre line in span-wise (three rows, Δz = 15 mm) and stream-wise ($0.12 \leq x/c \leq 0.57$, Δx = 10 mm) direction. By means of this 'baseline configuration', the general development of TS waves up to M = 0.4 was investigated. The highly sensitive sensors applied are able to detect even the tiniest TS waves in their early linear stage. The SHW was especially designed for experiments on AWC [1]. A principle sketch of a SHW set-up is shown in Fig. 3a. A platinum coated tungsten hot wire ($\varnothing\, 5\,\mu$m) is welded over a narrow cavity (0.075-0.1 mm) flush to the wing's surface. The SHW are usually operated in the constant-temperature mode (Constant-Temperature-Anemometry, CTA) with an overheat ratio up to 1.8. The reliability of the SHW was demonstrated by over 100 operating hours without any failures.

In Fig. 4, the power-spectra of transitional sensor signals are exemplarily displayed for Mach numbers 0.30, 0.35 and 0.40. With the convection velocity of the TS waves and the corresponding mean TS frequencies, the mean TS wavelength can be calculated as $\lambda_{TS} = c_{conv}/f_{TS}$ and actuator dimensions can be deduced. As can be seen, the instable domain shifts to higher frequencies with increasing flow

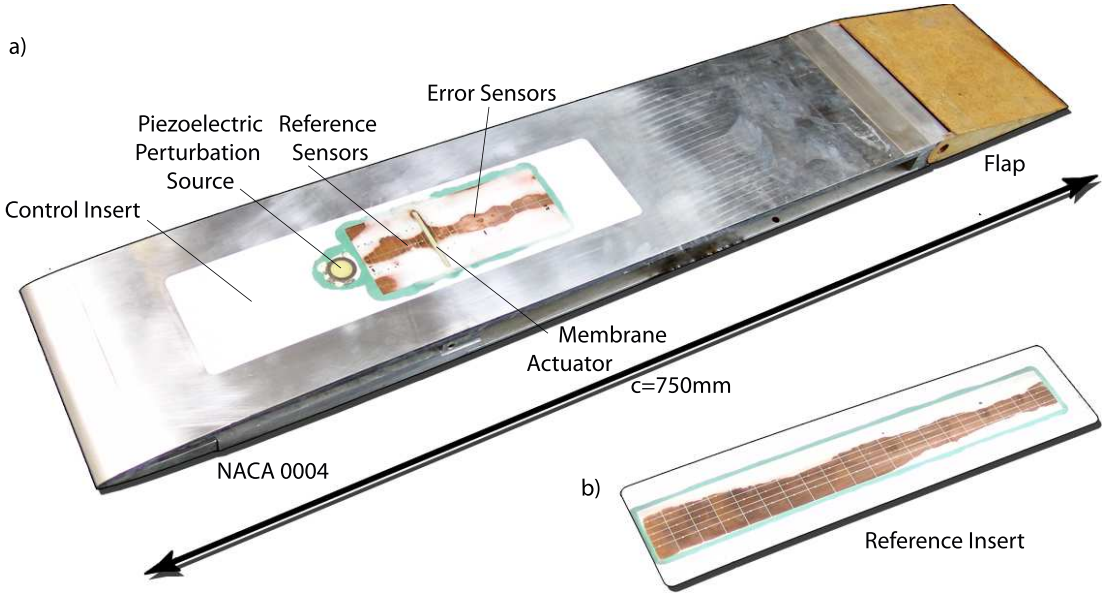

Fig. 2 Generic wing model with **a)** control- and **b)** reference-insert

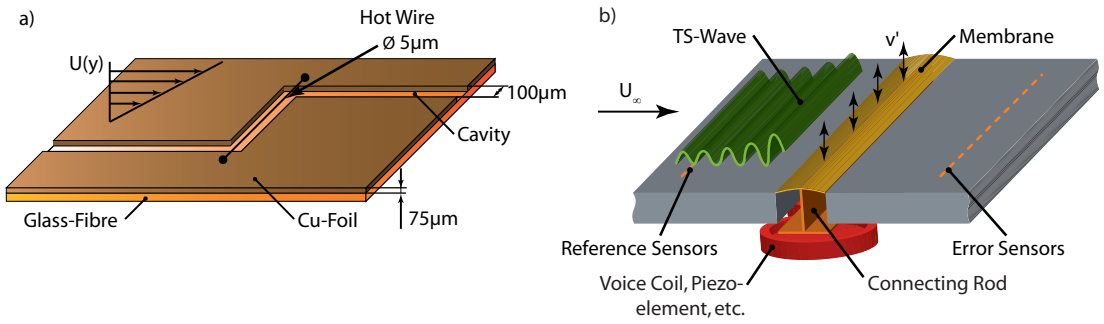

Fig. 3 Principle of a **a)** surface hot wire and **b)** membrane actuator

velocity which leads to smaller dimensions of the actuator.

Another plate insert – control insert – consists of a span-wise arranged SHW array (x/c = 0.30), which is used as a reference-sensor to detect the oncoming TS waves in the control experiments. Downstream (x/c = 0.33), a two-dimensional zero-net-mass flux actuator is employed to introduce appropriate counter waves as oscillating velocity fluctuations perpendicular to the surface of the wing, Fig. 3b. A flush-mounted highly flexible membrane is driven through a T-shaped connecting rod by a voice-coil or a piezo-electric disc bender. The high receptivity of the boundary layer to this actuator arises due to the smooth modulation of the counter waves in the range of the natural TS wave number. The best results were obtained with a membrane depth of $t \approx 1/4\ \lambda_{TS}$. The control insert is completed by another span-wise SHW array downstream of the actuator which is used as an error-sensor (x/c = 0.36) for the control experiments.

In addition to the arrangement described above, a perturbation source is installed at x/c = 0.25 to introduce controlled artificial perturbations. Considering the fact that the perturbations introduced are known (in respect of their frequency and amplitude), it is possible to test and optimise the controller prior to the experiments with natural TS waves where neither fre-

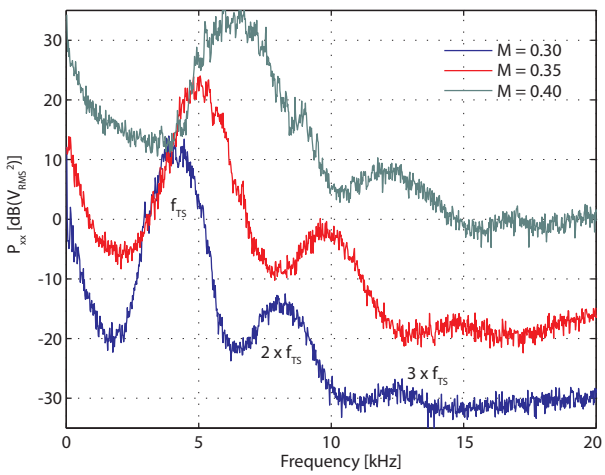

Fig. 4 Power-spectra at early TS amplification stages

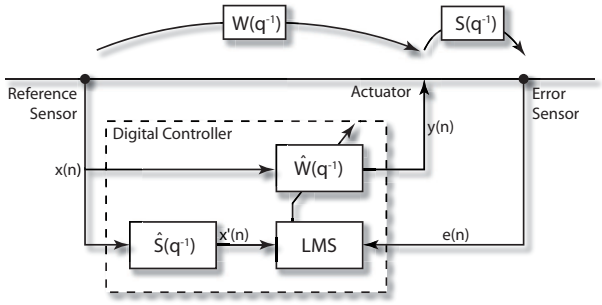

Fig. 5 Block diagram of a feed-forward AWC system (physical set-up)

quency and amplitude nor phase are known.

3 Control Strategy

Natural TS instabilities occur randomly as wave packets. Therefore, an effective damping can only be obtained by a closed-loop control algorithm working in real time. For several years, a feed-forward adaptive linear control algorithm performed by a fast Digital Signal Processor (DSP) has been applied successfully at TU Berlin [1, 4, 5]. The principle of this approach is shown in Fig. 5. $W(q^{-1})$ denotes the physical boundary layer transfer path of the TS waves. The purpose of the adaptive controller $\hat{W}(q^{-1})$ is to calculate (based on the reference-signal x(n)) an appropriate counter wave signal y(n). In order to cancel the TS wave at the position of the actuator, $\hat{W}(q^{-1})$ has to be adapted to ensure that it is an estimate of the physical path $W(q^{-1})$. Since $W(q^{-1})$ is the unknown system to be identified by the adaption algorithm, it is subsequently referred to as 'adaption path'.

The destructive interference of the counter wave signal propagated by the actuator and the TS wave, creates a 'zone of silence' in the vicinity of the error-sensor. The error-sensor measures the residual perturbations, which are used by the Least-Mean-Squares (LMS) algorithm for the adaption of the Finite Impulse Response (FIR) transfer function $\hat{W}(q^{-1})$ in order to minimize the signal power of the error-sensor e(n). Due to the signal delay and the re-amplification of the residual perturbations between the actuator and error-sensor, an estimation of the so called secondary path $\hat{S}(q^{-1})$ is mandatory. The filtering (filtered-x-LMS, FxLMS) of the reference-signal x(n) through $\hat{S}(q^{-1})$ is required by the fact that the output y(n) of the adaptive path $W(q^{-1})$ is physically filtered through $S(q^{-1})$. The secondary path $\hat{S}(q^{-1})$ comprises the digital to analogue converter, the power amplifier, the actuator, the physical behaviour of the boundary layer (receptivity, bandpass, amplification) from the actuator to the error-sensor, the error-sensor, the signal conditioner and the analogue to digital converter. Therefore, it even accounts for degeneration processes of single elements, e.g. the aging of the actuator.

Typical converged FIR filters modelling the secondary path $\hat{S}(q^{-1})$ and adaptive path $\hat{W}(q^{-1})$ are illustrated in Fig. 6.

The impulse responses of the FIR filters show the characteristics of a bandpass filter expressing the frequency selective amplification of TS waves. The delay of the wavy pulse is the propagation time modelled between the reference-sensor and the actuator of the TS disturbances.

The operating digital signal processor system (dSPACE, DS1005 PPC) has direct access to a 32-channel A/D converter (DS2003 A/D Board) and a 32-channel D/A converter (DS2103 D/A Board). The DS1005 features an IBM PowerPC

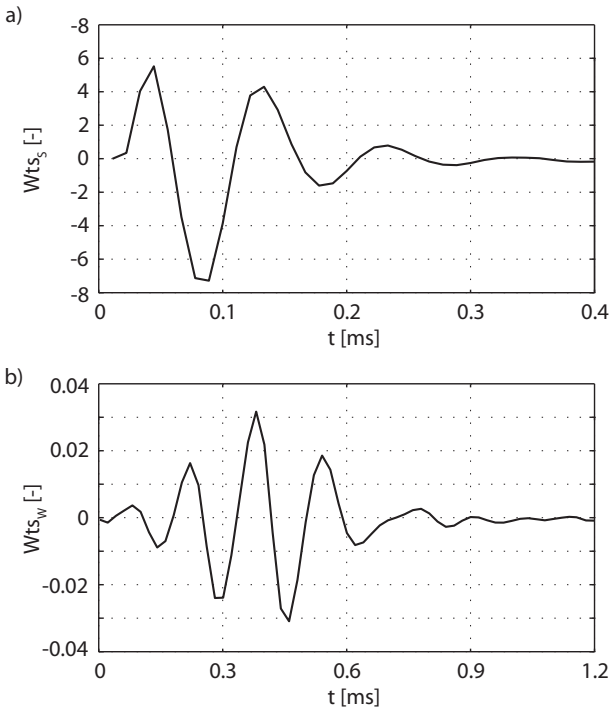

Fig. 6 Estimated filter weights of **a)** secondary path $\hat{S}(q^{-1})$ and **b)** adaptive path $\hat{W}(q^{-1})$

750GX running at 1 MHz. Usually, sampling rates of 60 kHz and impulse lengths of 0.4 ms for the secondary path and 1.2 ms for the adaptive path are employed for an effective TS wave cancellation. Higher sampling frequencies lead to an undesired "overfitted" transfer function and reduced cancellation rates. The programming is based on the Matlab Simulink Real-Time Interface as a link between the DSP hardware and the development software.

4 Results and Discussion

Due to the huge amount of test data all results are exemplarily discussed below for experiments conducted at M = 0.37.

Since the control strategy is based on an FxLMS algorithm, it can only model linear scenarios. Therefore, all paths which have to be estimated (amplifier, actuator, boundary layer, sensors, signal conditioner, etc.) have to follow linear characteristics. For this reason, the coherence-spectra between the reference- and error-sensor as well as between the actuator and error-sensor for the secondary path are of vital importance. High coherence values – especially in the fundamental TS instability range – from the basic requirements for a successful cancellation. The normalized coherence-spectrum is *one* in case of a fully linear dependency between the two signals tested, while a coherence of *zero* shows their independency.

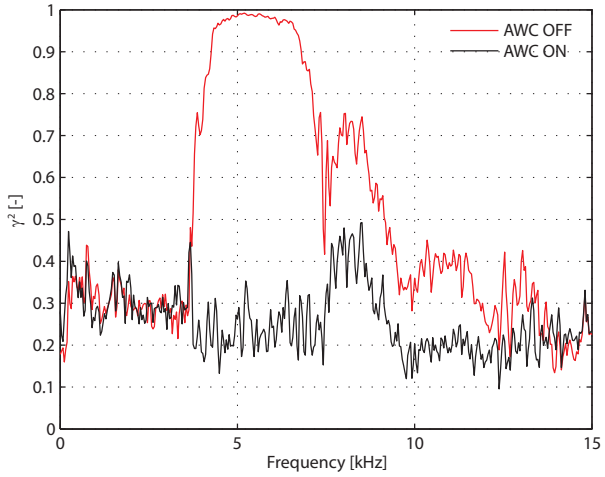

Fig. 7 Coherence-spectra between the reference- and error-sensor

Fig. 7 depicts the coherence-spectra for an operating and non-operating AWC system between the reference- and error-sensor. The stream-wise distance is about 15 mm, symmetrically up- and downstream to the actuator. In the frequency range of the fundamental TS instabilities for M = 0.37 ($3.6 \leq f_{TS} \leq 7.4$ kHz) the coherence reaches the high level of 95 to 98 %, which promises high cancellation rates. Relatively high coherence values are indicated in the overlap of the fundamental and the higher harmonic frequencies. Nevertheless, it is not possible to assign these frequencies to TS waves which will be proven by the power-spectrum of the error-sensor shown later. Presumably, this effect is driven by structure-borne noise and vibrations. In the range of the higher harmonic mode ($\approx$ 9-13 kHz), coherence values up to 0.4 are achieved, which indicates some cancellation potential. In contrast, the coherence distribution for

an operating AWC system is displayed in this figure as well. After the adaptive FxLMS algorithm is fully converged, the coherence is remarkably reduced in the fundamental TS frequency band. Even in the range of the first higher harmonic frequencies, a decrease of the coherence values becomes obvious. The already addressed high-coherence values close to the centre frequency of about 8.2 kHz are still distinct but reduced by approx. 0.3.

The success of the TS cancellation system becomes clear in the comparison of the power-spectra of the error-sensor for the cases of a running or non-running system. If AWC is operating, the power-spectra of the error-signal (Fig. 8a) show a remarkably reduced signal power in the frequency range of the fundamental TS instabilities compared to the case without AWC. A mean cancellation of about 20 dB can be observed in the fundamental TS frequency range ($3.6 \leq f_{TS} \leq 7.4$ kHz), which corresponds to a reduction of the TS amplitudes of about 90 %. In contrast, the reduction of the first higher harmonic mode between 9 and 13 kHz is limited to 2-3 dB. However, the fundamental mode accounts for the largest amplitudes of the instability signal, as Fig. 8b clearly shows. The scaled time-traces impressively demonstrate the cancellation effect. The remaining high-frequency perturbations are still obvious but of small amplitude. The peak in the power-spectrum at 2.9 kHz is caused by an acoustic tone which was observed during the experiments. Although it is an uncritical perturbation (the frequency of the perturbation is outside the instability mode and therefore damped), it was not possible to suppress this tone during the experiments.

While the power-spectrum of Fig. 8 is a long-term averaged result (measurement period 1 s), the spectrogram of Fig. 9 demonstrates that the cancellation affects instantaneously.

Fig. 9a shows the temporal distribution of the TS frequencies on the error-sensor for the non-operating cancellation system. As can be seen in Fig. 9b, the operating AWC system reduces the signal power of the error-sensor during the entire measurement period. The effect

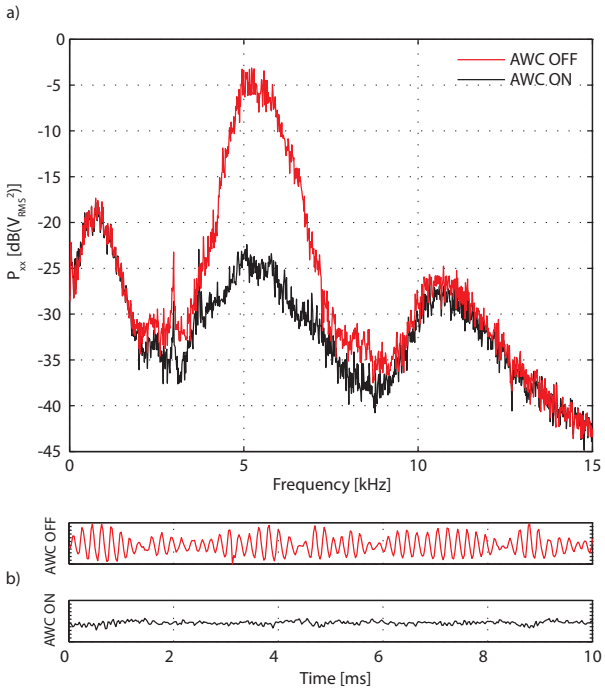

Fig. 8 a) Power-spectra and **b)** time-traces of the error-sensor for an active or inactive cancellation system

is stable in the long-term far beyond the period shown. Comparable to the power-spectrum, the cancellation of TS instabilities in the fundamental TS range is impressive while there is hardly any effect at the higher harmonic mode. Additionally, in case of an operational cancellation system, broadband noise amplitudes become randomly obvious throughout the frequency range and measurement period.

Following Elliott and Nelson [3] on the assumption that – if AWC is operating – only uncorrelated noise remains, an estimation for the optimum cancellation D can be formulated: $D = 1 - \gamma^2$ and $D[dB] = -20\log(1-\gamma^2)$, respectively. Therefore, based on the coherence-spectrum of the non-operating AWC system (Fig. 7), an estimation of the cancellation amplitude can be performed, Fig. 10.

The strictly linear approach estimates a cancellation rate of about 33 dB in the centre frequency of the fundamental mode and 3 to 4 dB of the first higher harmonic frequency. The cancellation prediction in the range of the over-

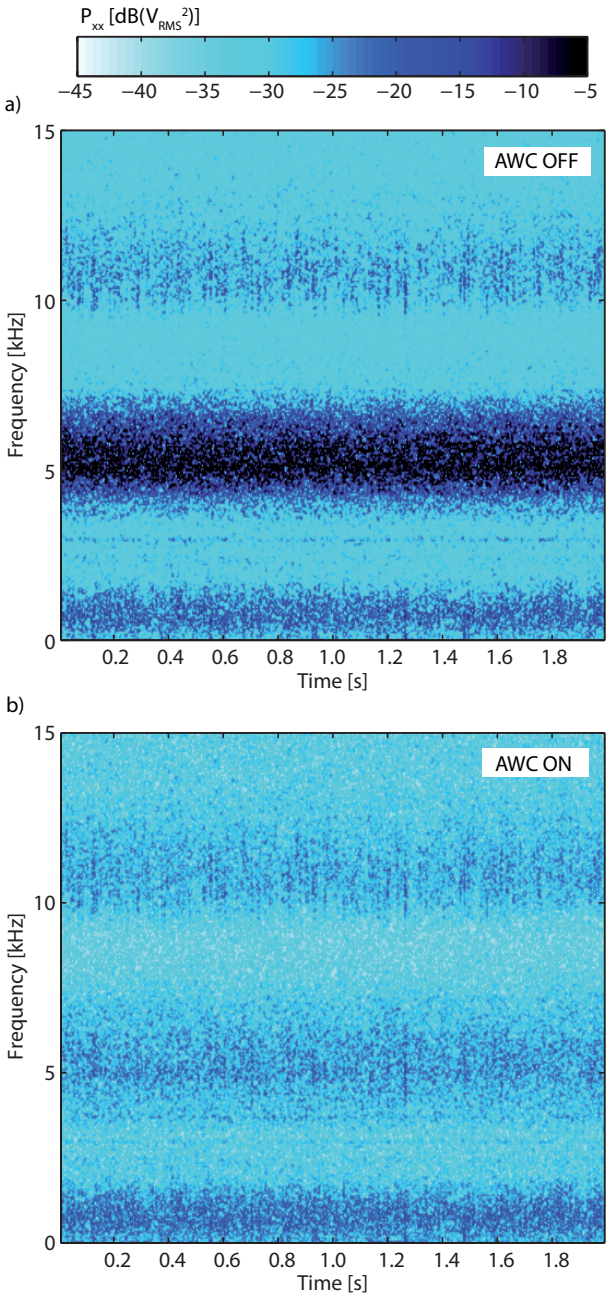

Fig. 9 Spectrogram of the error-sensor for an **a)** active or **b)** inactive cancellation system

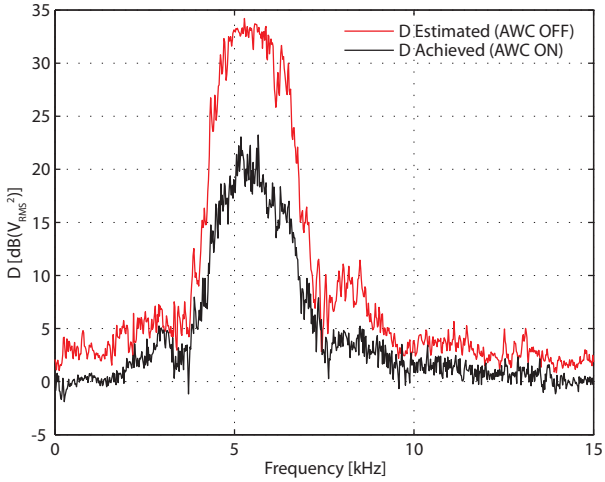

Fig. 10 Comparison of the estimated and achieved cancellation factor D

lap of the fundamental and higher harmonic frequencies results from the high coherence levels which are not assigned to flow signals. In comparison to this estimation, the cancellation rates achieved are indicated as well. The cancellation achieved is the difference of the power-spectra of the error-sensor for the cases of an operating and non-operating controller. In the range of the centre-frequency of the fundamental TS instability ($3.6 \leq f_{TS} \leq 7.4$ kHz) the estimated cancellation is about 15 dB higher than the values achieved. The estimated 5 dB in the range of the first higher harmonic mode ($9 \leq f_{TS} \leq 13$ kHz) failed almost completely. Due to the fact that the estimation is merely based on linear assumptions, the result has to be handled with care. The simple existence of a higher harmonic mode is evidence enough that the range of linear amplification of the TS waves is exceeded.

The spatial transition delay becomes particularly clear on the basis of the time-traces, Fig. 11. Fig. 11a shows the TS amplification for a non-operating actuator. The amplitude increase in the downstream direction results in a strong distortion of the typical wavy TS signal for the last two sensors plotted. In contrast, Fig. 11b displays the TS amplification upstream of the actuator and a strongly decreased amplitude downstream. The reference- and error-sensors used are the sensors directly in front of and behind the actuator, respectively. In addition to the time-traces, Fig. 11c summarizes the RMS distribution in stream-wise direction. In case of an operational cancellation system, the RMS value on the last sensor is decreased down to 18 % in comparison to a non-operational system. At the same time, the RMS value of the reference-sensor is increased in com-

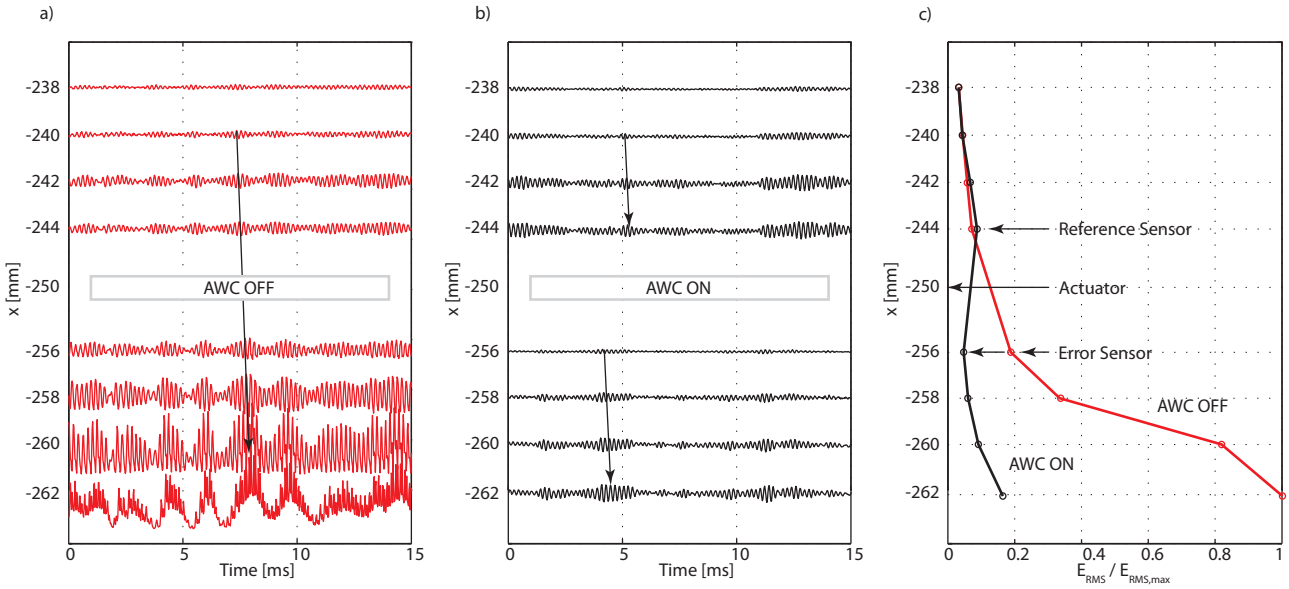

Fig. 11 Time-traces for a **a)** non-operating, **b)** operating controller and **c)** stream-wise RMS distribution for M = 0.37

parison to an inactive controller. This is caused by the undesired actuator effect upstream while introducing a counter wave.

5 Conclusion

A test rig consisting of an actuator, sensors and a controller was successfully designed and applied under compressible flow conditions at M = 0.37. The sensors used are surface hot wires, the actuator is a voice-coil driven membrane actuator. Finally, an FxLMS algorithm autonomously adapted a transfer function for the adaptive path between the reference-sensor and actuator in real time. The adaptive controller achieves a powerful cancellation of naturally occurring two-dimensional TS instabilities on an unswept wing. It enables a local TS amplitude reduction of about 90 % on the error-sensor.

Further experiments will deal with oblique running TS waves which requires an even more sophisticated control system. Therefore, an optimisation process of the controller will be performed. The AWC scheme of Fig. 5 works well for broadband and narrowband perturbed signals, but it suffers from an undesired feedback from the actuator to the reference-sensor. If feedback-neutralizing techniques are used, a further transfer function modelling the feedback path is required. Additionally, an implementation of a pre-noise filter for the reference signal is planned. This function utilizes two reference signals instead of the standard method which allows just one reference signal for the adaptive controller.

Acknowledgments

The work on Active Wave Control was funded by AIRBUS within the AIRNET project "Control of Aerodynamic Flows for Environmentally Driven Aircraft" (CAFEDA) and by the European Commission within the project "Aerodynamic Validation of Emission Reducing Technologies" (AVERT).

Copyright Statement

permission for the publication and distribution of their paper as part of the ICAS2008 proceedings or as individual off-prints from the proceedings.

References

[1] Baumann, M; Sturzebecher, D.; Nitsche, W.: Active Control of TS-Instabilities on an Unswept Wing. In: Laminar-Turbulent Transition, Springer, Eds. Fasel, H.; Saric, W.S.; pp. 155–160, 1999, ISBN 978-3-540-67947-9

[2] Burgess, J.C.: Active adaptive sound control in a duct: A computer simulation. In: The Journal of the Acoustical Society of America, Vol. 70, Issue 3, pp. 715–726, 1981

[3] Elliott, S.J.; Nelson, P.A.: Active Noise Control. In: IEEE Signal Processing Magazine, Vol. 10, Issue 4, pp. 12–35, 1993, ISSN 1053-5888

[4] Engert, M.; Pätzold, A.; Becker, R; Nitsche, W.: Active Cancellation of Tollmien-Schlichting Instabilities in Compressible Flows Using Closed-Loop Control. In: IUTAM Bookseries, Vol. 7, IUTAM Symposium on Flow Control and MEMS, Springer, Eds. Morrison, J.F.; Birch, D.M.; Lavoie, P.; pp. 319–331, 2008, ISBN 978-1-4020-6857-7

[5] Sturzebecher, D; Nitsche, W.: Active Control of Boundary-Layer Instabilities on an Unswept Wing. In: Recent Results in Laminar-Turbulent Transition, NNFM 86, Springer, Eds. Wagner, S.; Klocker, M.; Rist, U.; pp.169-202, 2003, ISBN 978-3-5404-0490-3

[6] Widrow, B.; Schur, D.; Shaffer, S.: On Adaptive Inverse Control. Proc. of the 15th Asilomar Conf. on Circuits, Systems and Computers, Pacific Grove, CA, pp. 185–195, Nov. 1981